J Nanostruct 13(3): 889-897, Summer 2023

RESEARCH PAPER

Study of the Optical, Structural and Adsorption Properties of Tellurium Oxide Nanoparticles and Graphene Nanosheets Prepared by Q-Switched Nd-YAG Pulsed Laser

Ghusoon Saeed [1], Mohammed H. K. AL- Mamoori [1], and Kaiser N. Madluim [2]*

[1] *Department of laser physics, College of Science for Woman, Babylon University, Hilla, Babil, Iraq*

[2] *Department of human anatomy, College of Medicine, University of Babylon, Hilla, Babylon, Iraq*

ARTICLE INFO

Article History:
Received 11 March 2023
Accepted 15 May 2023
Published 01 July 2023

Keywords:
Adsorption application
Graphene Nanosheets
Laser ablation
Tellurium Oxide Nanoparticles

ABSTRACT

Tellurium oxide nanoparticles (TeO_2NPs) and graphene nanosheets (GNS) were synthesized using a Q-Switched Nd-YAG Pulsed Laser in Liquid (PLAL) with a wavelength of 1064 nm, number of pulses 500, an energy per pulse of 80 mJ, a frequency of 6 Hz, and a pulse duration of 10 nsec. X-ray diffraction, FTIR, scanning electron microscopy (SEM), EDX, and UV-Vis Spectroscopy were all used to analyze TeO_2NPs and GNS. TeNPs were produced with a crystallite size of 39.6 nm. All of the reflections peaks can be indexed on a tetragonal α-TeO_2. XRD results show obtaining graphene nanosheet (GNS) from graphite using pulsed laser ablation in liquid. SEM results showed that spherical nanoparticles were obtained, and it was noted that there were some agglomerates with an average particle size of 65 nm. This is for TeO_2NPs, as for graphene, it was observed that graphene sheets were obtained. EDX results showed the presence of some impurities in the samples prepared for TeO_2NPs and GND. The results of FTIR showed that there is an absorption band at 561.5 cm1 for TeO_2NPs and 1643 cm^{-1} for graphene, respectively. The UV-visible spectroscopy results showed that there is a peak absorption at 292 nm with an energy gap of 1.4 eV for TeO_2NPs and 266 nm for graphene sheet, respectively. The adsorption results showed that graphene sheets have a high ability to adsorb methylene blue dye (MB) with an efficiency of up to 68.7% at the time of 15 seconds, while TeNPs enhanced the absorption in the visible region, and this indicates the possibility of using TeNPs with MB dye mixture in the manufacture of solar cells.

How to cite this article
Saeed G., AL- Mamoori M H., Madluim K N. Study of the Optical, Structural and Adsorption Properties of Tellurium Oxide Nanoparticles and Graphene Nanosheets Prepared by Q-Switched Nd-YAG Pulsed Laser. J Nanostruct, 2023; 13(3):889-897.
DOI: 10.22052/JNS.2023.03.030

INTRODUCTION

Nanoscience and nanotechnology are concepts used to describe the universe of "extremely small materials" (10^{-9} meters) that have a wide range of applications in sorts like energy, chemistry, biomedicine, environmental engineering, material science, optoelectronics, and life science [1]. Nanostructures do, in fact, exhibit unique capabilities (size-dependent optical, catalytic, electrical, and mechanical properties, for example [2]. Nanoscale materials can be used in a variety of applications due to their unique physical-chemical features (large surface energy, spatial confinement, and high surface to volume ratio). The building blocks of existing nanomaterials, nanoparticles (NPs), occur in a range of shapes. creation of a wide range of nanostructures [1].

* *Corresponding Author Email:*
Wsci.ghusoon.jaber.gsci54@student.uobabylon.edu.iq

Thin films and three-dimensional (3D) structures (super lattices) Tellurium (Te) is a p-type semiconductor with a band gap of (E_g = 0.35 eV) [3].It possesses a unique set of characteristics, including photoconductivity and catalytic activity in oxidation and hydration reactions[4], and nonlinear optical responses, thermoelectronic and high piezoelectronic[5]. Furthermore, solid tellurium combines with other elements to produce a variety of useful compounds, such as Bi_2Te_3, ZnTe, CdTe [6], However, the obtainability of low-dimensional tellurium (Te) nanostructures will almost certainly expose new applications or improve the performance of existing available devices in terms of the properties stated above [7]. As a result, the synthesis and characterization of tellurium nanoparticle fabrications piqued researchers' curiosity. It is, nevertheless, one of the rarest materials on the planet. Because of its scarcity, there is a significant desire to shape it as a nanoparticle, nanowire, or nanotube so that it can be used just where it is needed. As a result, it is a material of particular interest for a variety of applications, including solar cells [8]. The advantages of PLAL include the purity of the surface, which is free of chemical contamination, and the ease with which the particles may be collected and stored after synthesis. TeO_2 is a high-index refractive material that transmits in the infrared range, making it particularly intriguing for optical applications. TeO_2 has an energy gap of approximately 4.05 eV. It has also been shown to have Raman gain up to 30 times that of silicon dioxide, making it particularly effective in fiber optic amplification [9]. TeO_2 crystals are useful in acousto-optic systems owing to their advantageous photo-elastic characteristics, as well as their low light absorption, excellent optical homogeneity, and high optical damage resistance [10]. TeO_2 is an important material in both its amorphous and crystalline forms such as α-TeO2, with applications including optical storage material, X-ray detectors, laser devices, optical storage material, and gas sensors [11] and propane oxidation catalysts [12]. For the fabrication of TeO_2 thin films, several procedures such as reactive dip-coating, sputtering [13], and laser ablation have been utilized [14]. This work illustrated the activity of TeO_2NPs toward the removal of methyl blue dye from water. We have successfully produced TeO_2NPs in distilled water via PLA method. The morphological and optical properties were calculated for TeO_2NPs. Graphene is a proposed 2D-carbon lattice in the field of material research because of its unique chemical and physical features [15]. Graphene is a potential component in a variety of sectors, including solar cells [16], storage devices [17], sensors [18], energy conversion [19], and so on, due to its unique thermal and chemical stability, outstanding mechanical strength, superior electrical conductivity, large surface area. In recent years, a variety of techniques have been used to

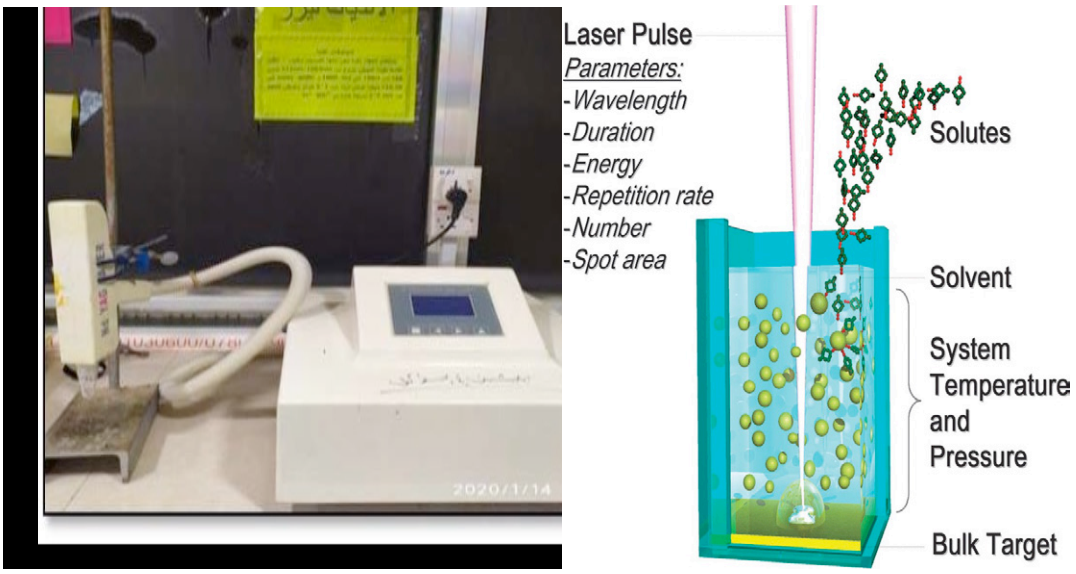

Fig. 1. Q-Switched Nd-YAG pulsed Laser Ablation in Liquids was used to create TeNPs and GNS in an experimental setup.

create graphene, including mechanical exfoliation of graphite [20], chemical vapor deposition (CVD)[21], orchemical reduction of graphene oxide (GO) [22]. Chemical reduction of graphene oxide is the most efficient way for preparing graphene in comparison to the other methods due to its low cost and large manufacturing capacity, as GO can be produced.

MATERIALS AND METHOD

Preparation of Te and Graphite Disc

A hydraulic piston was used to press (6 gm) of Te and (10 gm) of graphite powder at a pressure of 2 MP. After that, they were annealed in the oven for 24 hours.

Pulsed Laser Ablation in Liquids Syntheses of TeNPs and Graphene Nanosheet (GNS)

Tellurium oxide nanoparticles (TeO_2NPs) and graphene nanosheets (GNS) were generated as colloidal solutions by Q-Switched Nd-YAG pulsed laser ablation of a solid target of Te and Graphite powder in distilled water, with the Te and Graphite disc located in a glass container full with (10 ml) of distilled water. After that, a Q-Switched Nd-YAG pulsed laser (energy per pulse 80 mJ, number of pulses 500, λ =1064 nm, frequency (PRR) of 6 Hz, and pulse duration 10 ns) was used to irradiate the target. The colloidal liquid was then distillated onto the glass plate, which had previously been cleaned with water and alcohol, to create a thin film. It is then dry in an electric oven at a temperature of 25 ^{0}C. Finally, the thin film is ready to be measured using XRD, SEM, and EDX. The pulsed laser ablation method used to prepare the TeNPs and GNS is shown in Fig. 1.

RESULTS AND DISCUSSION

XRD measurements of TeO_2NPs and GNS samples

The crystal structure, distance between planes, crystalline size, and full width at half maximum (FWHM) were all studied using X-Ray Diffraction (XRD). Fig. 2 displays the TeO_2NPs XRD pattern at 2θ = 26. 7°, 33. 2°, and 61.9 °, which correspond to miller indices (011), (111), and (113) planes, respectively. The formation of TeNPs is indicated by these peaks, which is in agreement with the reference [23]. There is no additional peak, indicating that the synthetic material was of excellent crystalline purity. The Debye Scherrer equation (Eq.1) can be used to compute the crystallite size (D).

$$D = 0.89\,\lambda / (\beta \cos\theta)$$

β,θ and λ are the Full Width at Half Maximum (FWHM),the Bragg diffraction angle and X-ray wavelength respectively. the crystallite size of

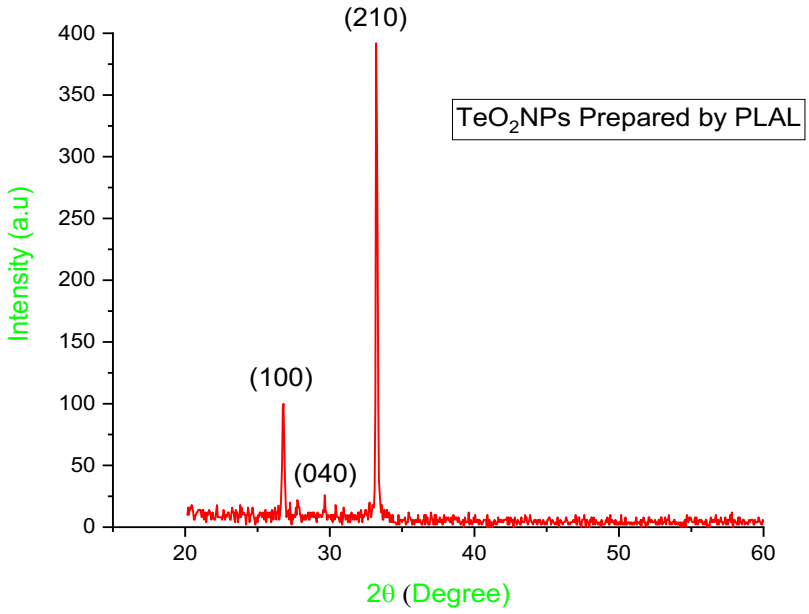

Fig. 2. XRD analysis of TeO_2NPs produced by pulsed laser ablation in distilled water.

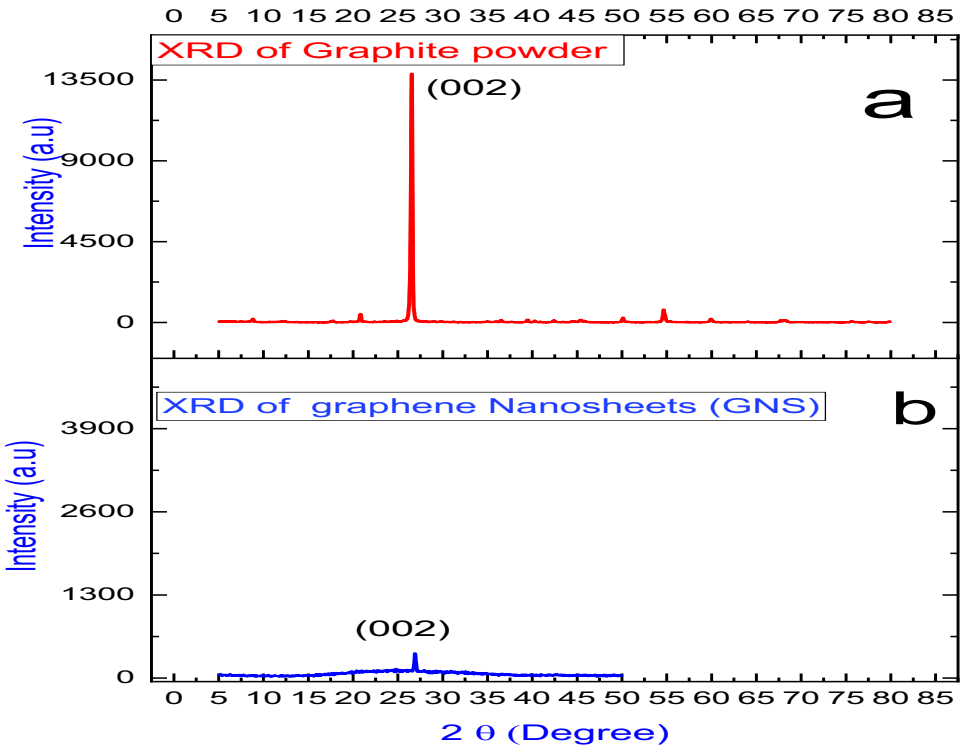

Fig. 3. XRD images of commercial graphite and graphene nanosheets (GNS) were obtained using pulsed laser ablation in pure water.

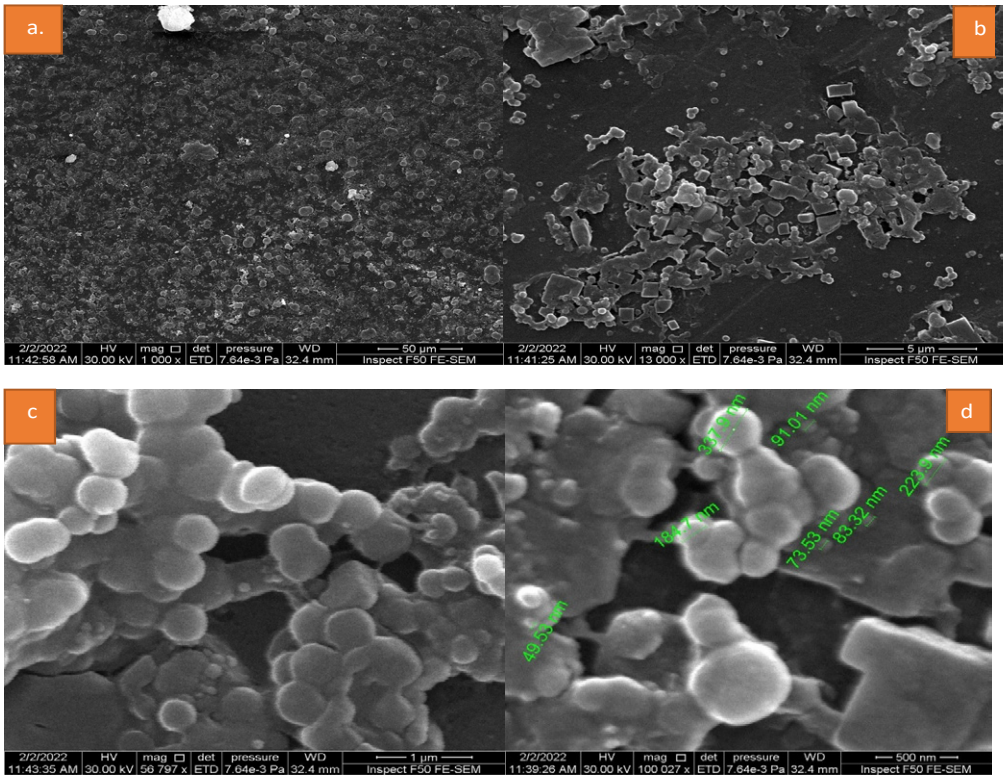

Fig. 4. SEM images of TeO_2NPs were prepared by pulsed laser ablation in distilled water .

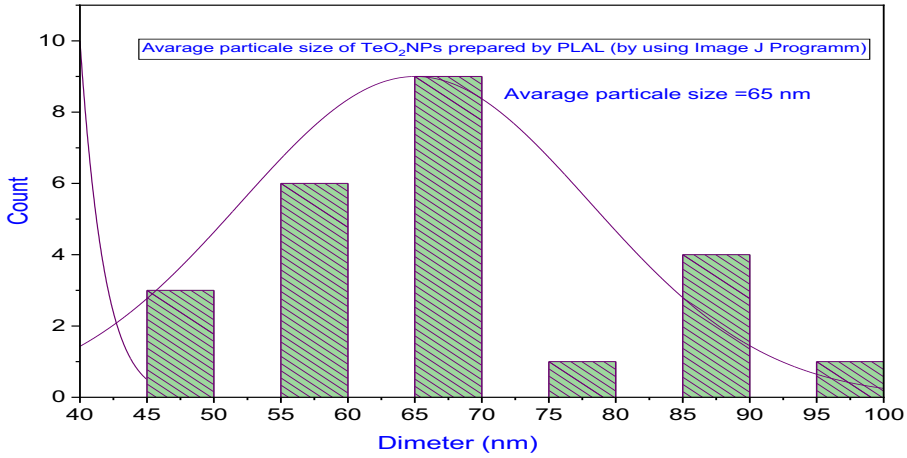

Fig. 5. Histograms representing the size distribution of the TeO_2NPs.

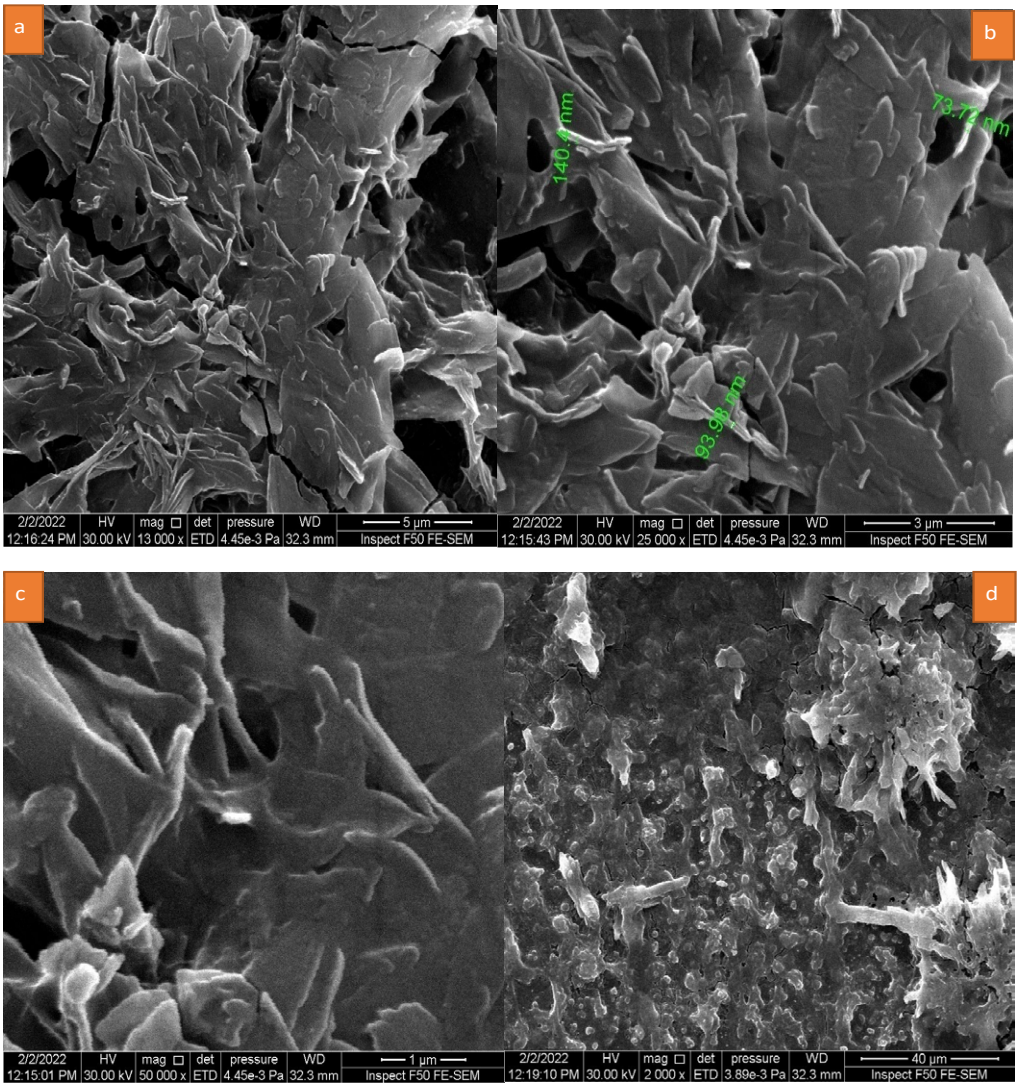

Fig. 6. Scanning Electron Microscopy of Graphene nanosheet (GNS)

TeO_2NPs had a value of 39.6 nm, which was calculated. Commercial graphite is liable for the reflection peak at 26.7°, which corresponds to 002, as seen in Fig. 3a. Fig. 3b indicates the presence of a smaller peak at 26.7°, corresponding to 002, which is very insignificant in comparison to the graphite peak, showing the production of graphene nanosheets (GNS).

Analyses of TeO_2NPs and GNS using Scanning Electron Microscopy (SEM) and EDX

The morphological parameters of the produced

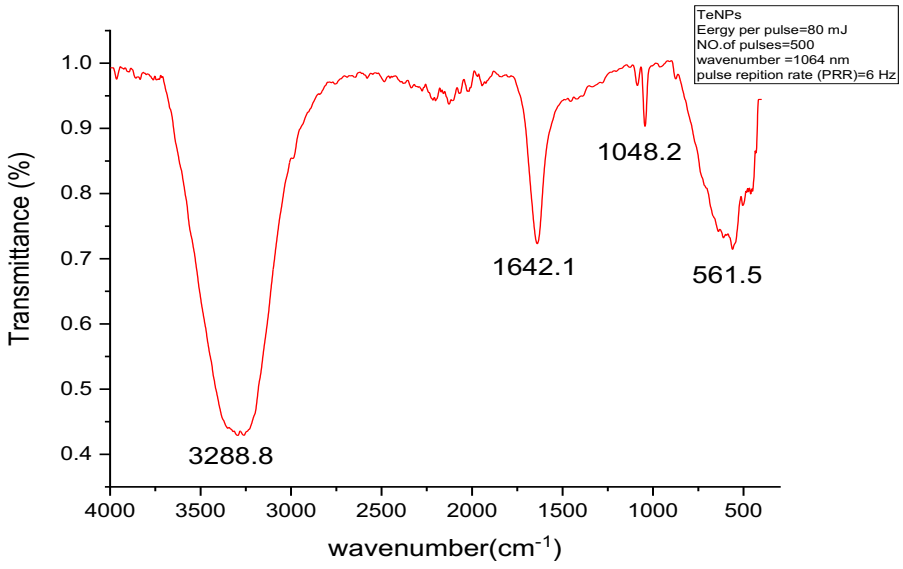

Fig. 7. FTIR spectrum of TeO_2NPs.

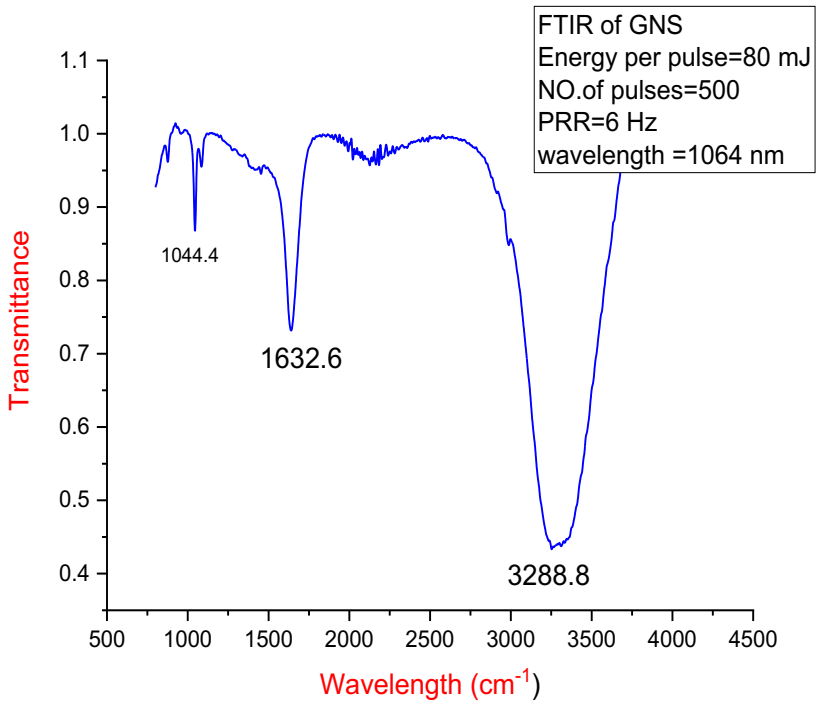

Fig. 8. FTIR spectrum of Graphene nanosheets (GNS)

materials were determined using SEM. The TeO_2NPs have a spherical shape, as seen in Figs. 4, a-d. There is some agglomeration of these particles at various locations. As indicated in Fig. 5, the average particle size is 65 nm. As demonstrated in Figs. 6 (a-d) graphite fragmentation with water using a pulse laser resulted in the formation of graphene nanosheets (GNS) and It is similar to what was mentioned in the reference [24, 25].

Fourier Transform Infrared Spectroscopy((FTIR)

The FTIR spectrum of TeO_2NPs and graphene nanosheets (GNS) powder was illustrated in Fig. 7 and (8), respectively. The absorption band at 561.5 cm^{-1}, 1048.2 cm^{-1}, 1642.1 cm^{-1}, and 3288.8cm^{-1} return to the stretching vibration of Te-O-T linkages, ester (COO) stretching vibrations,

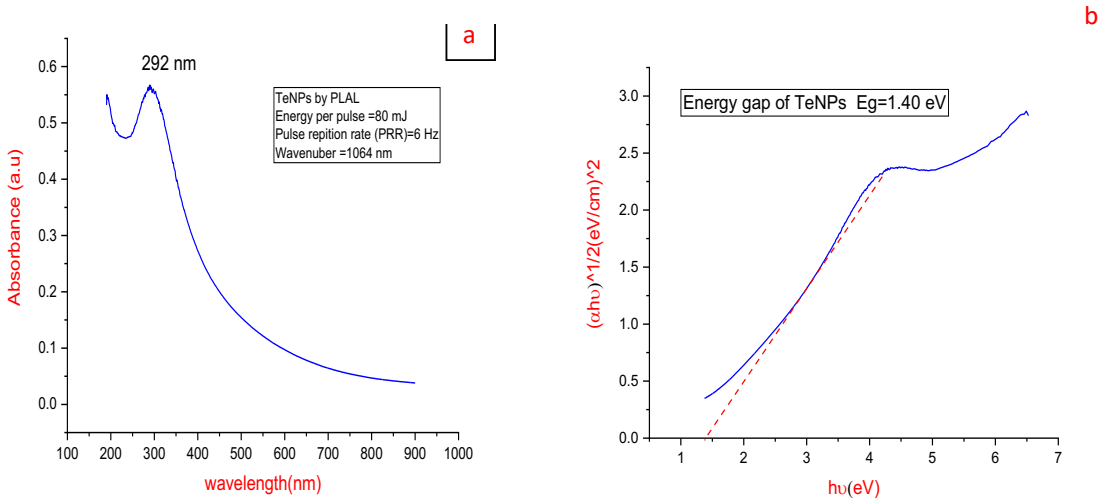

Fig. 9. UV-Vis spectra: a- TeO_2NPs , b-Energy gap of TeO_2NPs

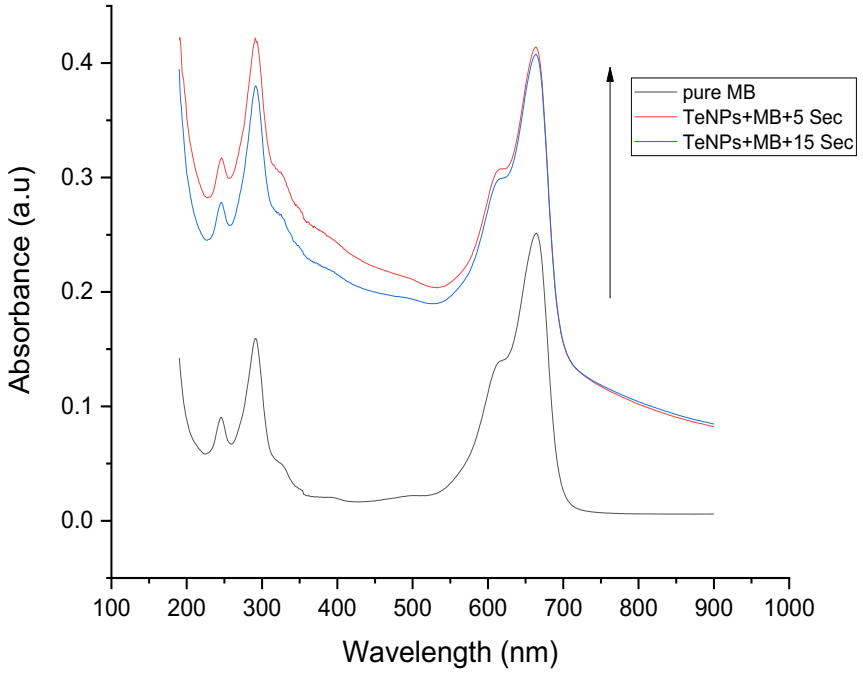

Fig. 10. UV – Vis spectrum of pure MB Dye and TeO_2NPs +MB mixture.

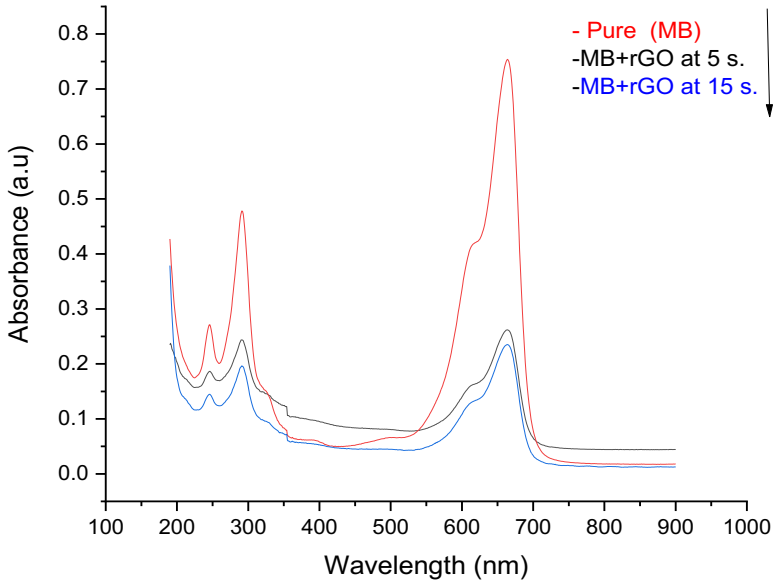

Fig. 11. UV – Vis spectrum of pure MB Dye and GNS+MB mixture.

C=O bonded, and O-H stretching vibrations, respectively [26, 27].

The FTIR spectrum of prepared GNS was illustrated in Fig. 8. The appeared intense peaks at (3288.8 cm^{-1}) were corresponding to stretching vibrations of hydroxyl (O-H) for water. The peak at (1632.6 cm^{-1}) refer to C=C stretching vibrations bond (skeletal vibrations from unoxidized graphitic domains). Stretching vibration peaks of C–O (alkoxy) are observed at 1044.4 cm^{-1} and it's close to the reference [28].

UV-Visible Absorption Spectroscopy:

The absorption peaks of TeO_2NPs and graphene nanosheet (GNS) are shown in Figs. 9a and b) respectively. Fig. 9a. At 292 nm, an absorption peak occurs as the valence band transitions to the conduction band. It returns to the production of TeO_2 nanoparticles [43]. According to the tauc plot, the energy gap for TeO_2 is 1.40 eV, as illustrated in Fig. 9. The transitions of the atomic C–C bonds cause the absorption peak at 265 nm, as illustrated in Fig. 9b, which agrees with the researcher's result in the reference [29].

Removing the Methylene Blue dye (MB) from the water by using the prepared TeO_2NPs and graphene nanosheets (GNS)

Methylene blue dye, which is utilized in textile and leather coloring, was removed using the TeO_2 NPs and GNS that had been prepared. 0.1 ml Methylene blue dye (M) was dissolved in 7.9 ml distilled water, and then 2.0 ml TeNPs and GNS were added to the methylene blue (MB) dye separately, and then the absorbance was calculated for each of the TeO_2NPs+MB and GNS+MB mixtures at two times t=5 s and t=15 s. Fig. 10 shows that TeNPs enhanced the absorbance of the methylene blue dye in the visible range. It is noted that the longer the time, the greater the absorbance intensity. This result indicates that it is not possible to use TeO_2NPs to remove pollutants, but this TeO_2NPs+MB mixture can be used in the manufacture of the solar cell because it enhances the absorption in the visible range.

As for Fig. 11 for the GNS+MB mixture, it indicates a high adsorption of MO dye due to the presence of GNS, with an adsorption efficiency of up to 65.3% and 68.7% for t = 5 s and t = 15 s, respectively.

CONCLUSION

TeO_2NPs and graphene nanosheets (GNS) were successfully generated in liquid utilizing a Q-Switched Nd-YAG pulsed laser (PLAL-Method). As indicated in UV-Visible absorption spectroscopy and FTIR investigations, the PLAL method is regarded a simple and important physical

method in the exfoliation of graphite in order to obtain graphene sheets. The prepared graphene nanosheet (GNS) has a high efficiency in the adsorption of MB dye, especially at time t = 15 s, with an adsorption efficiency of 68.7%. This is in contrast to the behavior of titanium nanoparticles (TeO_2NPs), as it enhances absorption in the visible range, and this behavior helps in the use of TeO_2NPs with MB dye in the manufacture of the solar cell better than using it in the adsorption process.

CONFLICT OF INTEREST

The authors declare that there is no conflict of interests regarding the publication of this manuscript.

REFERENCES

1. Microwaves in Nanoparticle Synthesis: Wiley; 2013.
2. Yuwen L, Wang L. CHAPTER 11.5. Nanoparticles and Quantum Dots. Handbook of Chalcogen Chemistry : New Perspectives in Sulfur, Selenium and Tellurium: Royal Society of Chemistry; 2013. p. 232-269.
3. Song J-M, Lin Y-Z, Zhan Y-J, Tian Y-C, Liu G, Yu S-H. Superlong High-Quality Tellurium Nanotubes: Synthesis, Characterization, and Optical Property. Crystal Growth & Design. 2008;8(6):1902-1908.
4. Loewen E. Investigation of polonium removal systems for lead-bismuth cooled fbrs. Prog Nuclear Energy. 2005;47(1-4):586-595.
5. Tangney P, Fahy S. Density-functional theory approach to ultrafast laser excitation of semiconductors: Application to the phonon in tellurium. PhRvB. 2002;65(5).
6. Kristl M, Drofenik M. Sonochemical synthesis of nanocrystalline mercury sulfide, selenide and telluride in aqueous solutions. Ultrason Sonochem. 2008;15(5):695-699.
7. Guisbiers G, Mimun LC, Mendoza-Cruz R, Nash KL. Synthesis of tunable tellurium nanoparticles. Semicond Sci Technol. 2017;32(4):04LT01.
8. Pokhrel D, Bastola E, Phillips AB, Heben MJ, Ellingson RJ. Aspect ratio controlled synthesis of tellurium nanowires for photovoltaic applications. Materials Advances. 2020;1(8):2721-2728.
9. Li Y, Fan W, Sun H, Cheng X, Li P, Zhao X. Structural, electronic, and optical properties of α, β, and γ-TeO_2. Journal of Applied Physics. 2010;107(9).
10. Salim ET, Ismail RA, Fakhri MA, Rasheed BG, Salim ZT. Synthesis of Cadmium Oxide/Si Heterostructure for Two-Band Sensor Application. Iranian Journal of Science and Technology, Transactions A: Science. 2018;43(3):1337-1343.
11. Siciliano T, Di Giulio M, Tepore M, Filippo E, Micocci G, Tepore A. Room temperature NO_2 sensing properties of reactively sputtered TeO_2 thin films. Sensors Actuators B: Chem. 2009;137(2):644-648.
12. Botella P, Concepción P, Nieto JML, Moreno Y. The influence of Te-precursor in Mo-V-Te-O and Mo-V-Te-Nb-O catalysts on their catalytic behaviour in the selective propane oxidation. Catal Today. 2005;99(1-2):51-57.
13. Lecomte A, Bamière F, Coste S, Thomas P, Champarnaud-Mesjard JC. Sol–gel processing of TeO_2 thin films from citric acid stabilised tellurium isopropoxide precursor. J Eur Ceram Soc. 2007;27(2-3):1151-1158.
14. Khalef WK, Marzoog TR, Faisal AD. Synthesis and characterization of tellurium oxide nanoparticles using pulse laser ablation and study their antibacterial activity. Journal of Physics: Conference Series. 2021;1795(1):012049.
15. Lee C, Wei X, Kysar JW, Hone J. Measurement of the Elastic Properties and Intrinsic Strength of Monolayer Graphene. Science. 2008;321(5887):385-388.
16. Wang H, Sun K, Tao F, Stacchiola DJ, Hu YH. 3D Honeycomb-Like Structured Graphene and Its High Efficiency as a Counter-Electrode Catalyst for Dye-Sensitized Solar Cells. Angew Chem Int Ed. 2013;52(35):9210-9214.
17. Zhuang XD, Chen Y, Liu G, Li PP, Zhu CX, Kang ET, et al. Conjugated-Polymer-Functionalized Graphene Oxide: Synthesis and Nonvolatile Rewritable Memory Effect. Adv Mater. 2010;22(15):1731-1735.
18. Fan Y, Liu J-H, Lu H-T, Zhang Q. Electrochemical behavior and voltammetric determination of paracetamol on Nafion/TiO_2–graphene modified glassy carbon electrode. Colloids Surf B Biointerfaces. 2011;85(2):289-292.
19. Chen T, Dai L. Carbon nanomaterials for high-performance supercapacitors. Mater Today. 2013;16(7-8):272-280.
20. Jiang Z, Li Q, Chen M, Li J, Li J, Huang Y, et al. Mechanical reinforcement fibers produced by gel-spinning of poly-acrylic acid (PAA) and graphene oxide (GO) composites. Nanoscale. 2013;5(14):6265.
21. Hu G, Jing M, Wang D-W, Sun Z, Xu C, Ren W, et al. A gradient bi-functional graphene-based modified electrode for vanadium redox flow batteries. Energy Storage Materials. 2018;13:66-71.
22. Stankovich S, Dikin DA, Piner RD, Kohlhaas KA, Kleinhammes A, Jia Y, et al. Synthesis of graphene-based nanosheets via chemical reduction of exfoliated graphite oxide. Carbon. 2007;45(7):1558-1565.
23. Youness F, Jaafar A, Tehrani A, Bilbeisi RA. Functionalised electrospun membranes (TETA-PVC) for the removal of lead(ii) from water. RSC Advances. 2022;12(38):24607-24613.
24. Aziz HM, Al-Mamoori MHK, Aboud LH. Synthesis and Characterization of Tio2-Rgo Nanocomposite by Pulsed Laser Ablation in Liquid (PLAL-Method). Journal of Physics: Conference Series. 2021;1818(1):012206.
25. Al-Nafiey A, Al-Mamoori MHK, Alshrefi SM, shakir AK, Ahmed RT. One step to synthesis (rGO/Ni NPs) nanocomposite and using to adsorption dyes from aqueous solution. Materials Today: Proceedings. 2019;19:94-101.
26. Zare B, Faramarzi MA, Sepehrizadeh Z, Shakibaie M, Rezaie S, Shahverdi AR. Biosynthesis and recovery of rod-shaped tellurium nanoparticles and their bactericidal activities. Materials Research Bulletin. 2012;47(11):3719-3725.
27. Islamic Republic of Iran: 1920 to Present: Middle East. Cultural Sociology of the Middle East, Asia, and Africa: An Encyclopedia: SAGE Publications, Inc.; 2012.
28. Rattana, Chaiyakun S, Witit-anun N, Nuntawong N, Chindaudom P, Oaew S, et al. Preparation and characterization of graphene oxide nanosheets. Procedia Engineering. 2012;32:759-764.
29. Amari A, Al Mesfer MK, Alsaiari NS, Danish M, Alshahrani AM, Tahoon MA, Rebah FB. Electrochemical and Optical Properties of Tellurium Dioxide (TeO_2) Nanoparticles. International Journal of Electrochemical Science. 2021;16(2):210235.